THE JOURNAL OF BIOLOGICAL CHEMISTRY VOL. 286, NO. 14, pp. 12627–12639, April 8, 2011

Functional Roles of a C-terminal Signaling Complex of Ca_V1 Channels and A-kinase Anchoring Protein 15 in Brain Neurons*[S]

Received for publication, August 13, 2010, and in revised form, January 6, 2011 Published, JBC Papers in Press, January 11, 2011, DOI 10.1074/jbc.M110.175257

Misty R. Marshall, John Patrick Clark III[1], Ruth Westenbroek[1], Frank H. Yu[1], Todd Scheuer, and William A. Catterall[2]

From the Department of Pharmacology, School of Medicine, University of Washington, Seattle, Washington 98195-7280

Regulation of $Ca_V1.2$ channels in cardiac myocytes by the β-adrenergic pathway requires a signaling complex in which the proteolytically processed distal C-terminal domain acts as an autoinhibitor of channel activity and mediates up-regulation by the β-adrenergic receptor and PKA bound to A-kinase anchoring protein 15 (AKAP15). We examined the significance of this distal C-terminal signaling complex for $Ca_V1.2$ and $Ca_V1.3$ channels in neurons. AKAP15 co-immunoprecipitates with $Ca_V1.2$ and $Ca_V1.3$ channels. AKAP15 has overlapping localization with $Ca_V1.2$ and $Ca_V1.3$ channels in cell bodies and proximal dendrites and is closely co-localized with $Ca_V1.2$ channels in punctate clusters. The neuronal AKAP MAP2B, which also interacts with $Ca_V1.2$ and $Ca_V1.3$ channels, has complementary localization to AKAP15, suggesting different functional roles in calcium channel regulation. Studies with mice that lack the distal C-terminal domain of $Ca_V1.2$ channels ($Ca_V1.2\Delta DCT$) reveal that AKAP15 interacts with neuronal $Ca_V1.2$ channels via their C terminus *in vivo* and is co-localized in punctate clusters of $Ca_V1.2$ channels via that interaction. $Ca_V1.2\Delta DCT$ neurons have reduced L-type calcium current, indicating that the distal C-terminal domain is required for normal functional expression *in vivo*. Deletion of the distal C-terminal domain impairs calcium-dependent signaling from $Ca_V1.2$ channels to the nucleus, as shown by reduction in phosphorylation of the cAMP response element-binding protein. Our results define AKAP signaling complexes of $Ca_V1.2$ and $Ca_V1.3$ channels in brain and reveal three previously unrecognized functional roles for the distal C terminus of neuronal $Ca_V1.2$ channels *in vivo*: increased functional expression, anchoring of AKAP15 and PKA, and initiation of excitation-transcription coupling.

Voltage-gated calcium channels of the Ca_V1 subfamily conduct L-type calcium currents that transduce cell-surface depolarization into calcium transients and initiate excitation-contraction coupling, excitation-secretion coupling, protein phosphorylation, and gene regulation (1–5). Calcium influx via postsynaptic Ca_V1 channels supports sustained phosphorylation of cAMP response element-binding protein (CREB)[3] and CREB-dependent gene expression in hippocampal neurons (6–13).

Functional Ca_V1 channels are multimeric complexes composed of pore-forming α_1 and associated $\alpha_2\delta$, β, and in some cases, γ subunits (14–19). These channels have an extended C terminus containing many protein interaction sites for regulation (5). In brain, Ca_V1 channels are composed of 70% $Ca_V1.2$ and 22% $Ca_V1.3$ with minor contributions from other Ca_V1 channels, as indicated by immunoprecipitation with specific antibodies (20). $Ca_V1.2$ and $Ca_V1.3$ channels are primarily localized in the soma and proximal dendrites (20, 21).

The β-adrenergic pathway activates cAMP-dependent protein kinase (PKA) and increases the activity of Ca_V1 channels in skeletal and cardiac myocytes and neurons (1–5, 22, 23). PKA-mediated regulation of $Ca_V1.2$ channels in cardiac and skeletal muscle requires a plasma membrane-targeted A-kinase anchoring protein (AKAP15) that binds directly to $Ca_V1.1$ and $Ca_V1.2$ channels via a leucine zipper (LZ) motif in the distal C-terminal region, thereby positioning PKA in close proximity to its phosphorylation targets (24–27). The LZ-like sequences in the distal C-terminal domains of cardiac, skeletal muscle, and neuronal Ca_V1 channels are well conserved, suggesting that AKAP15 may target $Ca_V1.2$ and $Ca_V1.3$ channels in brain through a similar motif. In contrast to the results on AKAP15 in skeletal and cardiac myocytes, a previous study showed that the AKAP microtubule-associated protein 2B (MAP2B) associates with $Ca_V1.2$ channels in brain (28). In the experiments presented here, we have further defined the C-terminal signaling complex of $Ca_V1.2$ and $Ca_V1.3$ channels *in vivo*. We found that AKAP15 and β_2ARs are components of $Ca_V1.2$ and $Ca_V1.3$ channel signaling complexes in the brain. MAP2B and AKAP15 have complementary localization suggesting that they interact with distinct subsets of Ca_V1 channels in neurons. Deletion of the distal C-terminal domain of $Ca_V1.2$ channels *in vivo* decreased L-type calcium currents, altered the localization of AKAP15, and impaired coupling of calcium channel activation to phosphorylation of CREB. These results show that AKAP15 anchors PKA to the distal C terminus of $Ca_V1.2$ and $Ca_V1.3$ channels in brain neurons *in vivo* and reveal three previously unrecognized functional roles for the distal C-terminal signaling complex of $Ca_V1.2$ channels in neurons *in vivo*: increased

* This work was supported, in whole or in part, by National Institutes of Health Grant Training Grants T32 GM07750 (to M. R. M.) and T3207332 (to J. P. C.) and Research Grants P01 HL44948, R01 HL85372, and R01 NS22625 (to W. A. C.).

[S] The on-line version of this article (available at http://www.jbc.org) contains supplemental Figs. 1 and 2.

[1] These authors contributed equivalently to this work and are listed alphabetically.

[2] To whom correspondence should be addressed. E-mail: wcatt@uw.edu.

[3] The abbreviations used are: CREB, cAMP response element-binding protein; LZ, leucine zipper; HBSS, Hanks' balanced salt solution; AKAP15, A-kinase anchoring protein 15; MAP2B, microtubule-associated protein 2B; SM, skim milk; β_2AR, β_2-adrenergic receptor.

functional expression, anchoring of AKAP15/PKA, and initiation of excitation-transcription coupling.

MATERIALS AND METHODS

Antibodies—Rabbit polyclonal anti-$Ca_V1.2$ (anti-CNC1) and anti-$Ca_V1.3$ (anti-CND1) and chicken polyclonal anti-$Ca_V1.2$ (anti-CNC1) were generated against amino acid sequences (29) in the intracellular loop betweens domains II and III of $Ca_V1.2$ and $Ca_V1.3$ channels as described (30, 31). An antibody against the distal C terminus (anti-CH2) was generated against residues 2051–2066 in the distal C terminus of $Ca_V1.2$ channels and characterized as described (32). Anti-AKAP15 antibodies and RII-biotin protein were prepared as described (26). Rabbit-HRP secondary antibody, streptavidin-HRP secondary antibody, and control antibodies (rabbit IgG) were purchased from Zymed Laboratories Inc. (South San Francisco, CA), and anti-phospho-CREB Ser^{133} and anti-phospho-ERK were from Millipore (Billerica, MA).

Preparation of Mouse Brain Membrane Proteins—All preparative steps were performed at 0–4 °C using prechilled solutions. Whole brains from 10-week-old C57Bl6 mice were homogenized in buffer containing 5 mM EDTA, 1 mM dithiothreitol, 50 mM Tris-Cl (pH 7.4), 0.32 M sucrose, and protease inhibitors. Homogenates were centrifuged at 1000 × *g* to remove debris, and membranes were collected by ultracentrifugation at 100,000 × *g* for 45 min. Membranes were solubilized in homogenization buffer containing either 2% digitonin or 0.5% Triton X-100 for 30 min with mixing by rotation, and insoluble material was removed by ultracentrifugation. All extracts contained the protease inhibitors pepstatin A (1 μM), benzamidine (100 μM), leupeptin (1 μM), aprotinin (0.3 μM), phenylmethanesulfonyl fluoride (1 mM), trypsin inhibitor (20 μg/ml), PefBloc SC (1 mM), and calpain inhibitors I and II (20 μg/ml each). Proteins that nonspecifically bind to Sepharose beads were removed by mixing mouse neuronal membrane extracts with protein A-Sepharose (5 mg) by rotation for 30 min at 4 °C. The precleared lysates were incubated with either 15 μg of affinity-purified anti-$Ca_V1.2$ channel antibody, 15 μg of affinity-purified anti-$Ca_V1.3$ channel antibody, or 15 μg of control nonimmune IgG. After 2 h of mixing at 4 °C, 5 mg of protein A-Sepharose was added for an additional 1 h. Immune complexes bound to Sepharose beads were sedimented by centrifugation and washed extensively. Samples were then extracted with 40 μl of SDS sample buffer and analyzed by SDS/PAGE on 8–16% gradient gels and immunoblotting. Each immunoprecipitation experiment was repeated at least four times.

Immunoblot Analysis—After separation by SDS-PAGE using 8–16% gels, proteins were transferred and blocked by incubation with 5% skim milk powder (5 M) in 20 mM Tris-HCl, 0.15 M NaCl (pH 7.4) (TBS) for 2 h or overnight. Blots were incubated with affinity-purified antibodies in 5% skim milk powder (SM-TBS) with anti-$Ca_V1.2$ (1:150 in SM-TBS), anti-$Ca_V1.3$ (1:100 in SM-TBS), or anti-β_2AR (1:50 in SM-TBS). For AKAP15 detection, immunoblots were probed with an anti-AKAP15 antibody (1:150 in SM-TBS) or the RII-biotin overlay assay (25), which detects all AKAPs. After several rinses, streptavidin-HRP was applied to visualize the AKAP interactions, and the resulting blots were developed with standard protocols. The blots were washed with TBS containing 0.05% Tween 20 (TBST) (three changes), incubated for 1 h with horseradish peroxidase-labeled donkey anti-rabbit antibody (Amersham Biosciences) or horseradish peroxidase-labeled protein-A, diluted 1:10,000 in SM-TBST, washed 5–6 times with TBST, and developed with ECL reagent.

Generation of $Ca_V1.2\Delta DCT$ Mice—A stop codon was inserted into the coding sequence of the *Cacna1c* gene encoding $Ca_V1.2$ channels at Gly-1796, where $Ca_V1.2$ channels are truncated *in vivo* (33). Germ line transmission of the mutated *Cacna1c* allele was confirmed for one of three chimeric mice, and the resulting progeny were backcrossed into C57Bl/6J for more than 10 generations to generate the $Ca_V1.2\Delta DCT$ animals used in this study. Wild-type and $Ca_V1.2\Delta DCT$ mutant animals were identified by PCR analysis of tail-tip DNA in a 24-μl reaction containing 2 μl of DNA (100 ng/μl), 0.2 μl of 25 mM dNTPs, 2.5 μl of 10× Taq buffer (Invitrogen), 0.5 μl of forward primer (FH258, CCCACTGCACATCAACAAGAC), 0.5 μl of reverse primer (FH254, GTCCTGTGTGGAAGACTCAAGGAG), 0.2 μl of Promega Taq polymerase (5 units/μl), 0.75 μl of 50 mM $MgCl_2$, and 19.3 μl of H_2O. Cycling conditions were 94 °C for 2 min, 35× (94 °C for 20 s, 62 °C for 30 s, 72 °C for 90 s), and 72 °C for 5 min followed by storage at 4 °C. The transgene produces a DNA product of 908 bp from all transgenic animals, which is further analyzed using an NcoI restriction digest to detect the NcoI restriction site in exon 44 that has been removed in $Ca_V1.2\Delta DCT$ mice. Wild-type mice show a DNA band of 702 bp, whereas $Ca_V1.2\Delta DCT$ mice show a DNA band of 908 bp. Heterozygous mice have both DNA bands.

Isolation of Hippocampal Neurons—Cultures of hippocampal neurons were prepared essentially as described previously (13). In brief, hippocampi were isolated from embryonic day 18 mice, and the CA1-CA3 region was dissected in Hanks' balanced salt solution containing 10 mM $MgCl_2$ (HBSS+Mg^{2+}). The dentate gyrus was removed to minimize inhibitory neurons in the cultures. The tissue was incubated in HBSS+Mg^{2+} containing 1 mg/ml activated papain (Worthington Biochemical, Freehold, NJ) at 37 °C for 30 min. The tissue was rinsed with HBSS+Mg^{2+} and dissociated to a single cell suspension by gentle passage through a 2-ml serological pipette, seeded onto 24-well plates coated with mouse laminin/poly-D-lysine, and maintained in neurobasal medium supplemented with B27 (Invitrogen). Cells were plated at 2×10^4 cells per well in 24-well tissue culture plates for immunocytochemistry or at 3×10^4 cells per plate for electrophysiology. Proliferation of non-neuronal cells was prevented by the addition of 0.08 mM fluorodeoxyuridine and 0.2 mM uridine (Sigma) from the third day in culture. Electrophysiological recordings were performed 10–16 days after plating.

Single-label Immunocytochemistry—Mice pregnant for 18 days were anesthetized and intracardially perfused with 4% paraformaldehyde. The brains of the pups were immediately removed, postfixed for 1 h, cryoprotected by sinking in 10% (w/v) and 30% (w/v) sucrose in 0.1 M sodium phosphate (pH 7.4 (PB)) at 4 °C for 72 h, and sectioned into 40-μm coronal and sagittal slices. The tissue sections were mounted on subbed slides and then processed for immunocytochemistry. The sections were rinsed in PB, fixed in 4% paraformaldehyde for 45

min, rinsed in PB for 5 min, rinsed in 0.1 M Tris buffer (pH 7.4 (TB)) for 15 min, rinsed in 0.1 M Tris-buffered saline (pH 7.4 (TBS)) for 15 min, and blocked in TBS containing 0.1% Triton X-100 and 10% normal goat serum. The sections were then incubated in anti-$Ca_V1.2$ (diluted 1:25), anti-$Ca_V1.3$ (diluted 1:25), anti-CH2 (diluted 1:15), or anti-AKAP15 (diluted 1:15) overnight at room temperature, rinsed in TBS, incubated in biotinylated goat anti-rabbit IgG (diluted 1:300, Vector Laboratories, Burlingame, CA) for 2 h at room temperature, rinsed in TBS, incubated in avidin D-fluorescein (diluted 1:300, Vector) for 2 h at room temperature, rinsed, and coverslipped using Vectashield.

Double-label Immunocytochemistry—Two-month-old C57Bl/6 mice were anesthetized and intracardially perfused with 4% paraformaldehyde in PB, and then the brains were removed, post-fixed, cryoprotected, and sectioned as described above. Free-floating slices were processed for immunocytochemistry using the method described previously (34). Tissue slices were incubated for 36 h at 4 °C with rabbit anti-$Ca_V1.2$ (1:25), rabbit anti-AKAP15 (1:25), mouse anti-MAP2B (1:200), chicken anti-$Ca_V1.2$ (1:25), chicken anti-β_2AR (1:25), or rabbit anti-$Ca_V1.3$ antibodies (1:25) diluted in 1% normal goat serum and 0.1% Triton X-100 in TBS. One bound primary antibody was detected using appropriate biotinylated IgG and avidin labeled with D-fluorescein, and the second bound primary antibody was detected with Alexa 555-labeled secondary antibody. Images were viewed using either the Leica SL or Bio-Rad MRC 600 confocal microscope in the W. M. Keck Imaging Facility. Control experiments were performed to confirm the specificity of labeling by omitting the primary antibody and using peptide-blocked antibodies as described previously (30, 35). Double labeling using two rabbit polyclonal antibodies was carried out as described (36).

Electrophysiology—Whole-cell Ba^{2+} currents (I_{Ba}) were recorded at room temperature from 10–14-day cultured neurons for total calcium channel currents (5 mM Ba^{2+}), non-L-type currents (in the presence of 10 μM nimodipine), and background currents (by substituting Co^{2+} for Ba^{2+}). The extracellular bath solution contained 140 mM tetraethylammonium-HCl, 2 mM $MgCl_2$, 5 mM $BaCl_2$, 10 mM Hepes, 10 mM glucose (pH 7.4), and 0.5 μM tetrodotoxin. Patch pipettes were filled with an intracellular solution containing 115 mM cesium methanesulfonate, 10 mM MgATP, 0.5 mM CsEGTA, 0.25 mM $CaCl_2$, 20 mM Hepes, 1 mM Tris GTP, 10 mM phosphocreatine, pH 7.21. Calcium channel currents were isolated by blocking Na^+ currents with tetrodotoxin and K^+ currents with tetraethylammonium and Cs^+. L-type currents were further distinguished with holding potentials selected to inactivate low voltage-activated calcium currents ($V_H = -50$ mV). To estimate the extent of current rundown, time-matched controls omitting nimodipine were recorded in parallel with the experimental cells. Currents were recorded with an Axopatch 200B amplifier (Molecular Devices, Union City, CA) and sampled at 50 kHz after filtering at 8 kHz. Data acquisition and command potentials were controlled by Pulse software (HEKA Electronik, Lambrecht, Germany), and data were stored for off-line analysis using Igor Pro (Wavemetrics, Lake Oswego, OR).

Measurement of CREB Phosphorylation—Dissociated CA1/3 hippocampal neurons from E18 wild-type and $Ca_V1.2\Delta DCT$ mice were maintained in culture for 8–14 days on a laminin/poly-D-lysine substrate (1:100 dilution, BD Biosciences) in Neurobasal A medium (Invitrogen) supplemented with B-27 (Invitrogen). Hippocampal neurons were stimulated by depolarization with solution containing 75 mM NaCl, 65 mM KCl, 2 mM $CaCl_2$, 1 mM $MgCl_2$, 25 mM Hepes, and 10 mM glucose. Sodium channels were blocked with 1 μM tetrodotoxin added the night before stimulation. P/Q- and N-type calcium currents were blocked with 1 μM ω-agatoxin IVA and 1 μM ω-conotoxin GIVA (Alomone Labs). *N*-Methyl-D-aspartate receptors were blocked with 100 μM D,L-2-amino-5-phosphonovaleric acid (Tocris, Ellisville, MO), and 40 μM 6-cyano-7-nitroquinoxaline-2,3-dione (CNQX) added 30 min before stimulation. Neurons were depolarized for 20 min and quenched with 1 mM sodium kynurenate and 10 mM $MgCl_2$. The neurons were immediately lysed in 2× boiling sample buffer, and proteins were separated by SDS-PAGE. Immunoblot analysis was performed with antibodies to phospho-CREB Ser^{133} (1:100), phospho-ERK (1:10,000), actin (1:5000), and CREB (1:200) to measure the level of phospho-CREB compared with total CREB.

Quantitative Image Analysis—Images were analyzed using Metamorph (Molecular Devices) and Igor Pro (Wavemetrics). For quantitation of punctate staining, puncta were counted in regions of interest in 2–4 tissue sections per condition from each of 3–4 experiments. In each experiment the number of puncta was normalized to the mean number of puncta counted in same-sized regions of interest from wild-type sections. Changes were compared by Student's *t* test as implemented in Excel (Microsoft, Redmond, WA). For analysis of nuclear fluorescence, whole nuclear regions of interest were taken from CREB and pCREB images, respectively, and mean pixel intensity was determined.

RESULTS

Interaction of AKAP15 with $Ca_V1.2$ Channels—AKAP15 targets PKA to an interaction site in the distal C terminus of L-type calcium channels in skeletal and cardiac muscle through LZ interactions (24, 37). The amino acid sequence of the AKAP binding domain in $Ca_V1.1$, $Ca_V1.2$, and $Ca_V1.3$ channels reveals high conservation of the hydrophobic LZ interaction motif (Fig. 1*A*), suggesting that AKAP15 may also target PKA to $Ca_V1.2$ and $Ca_V1.3$ channels in neurons. To examine if AKAP15 associates with $Ca_V1.2$ channels in brain, immunoprecipitation experiments were performed on solubilized extracts of adult mouse brain membranes prepared with either Triton X-100 or digitonin as detergent. These two detergents were selected because digitonin is a mild detergent that is unlikely to dissociate stable complexes, whereas Triton X-100 is more likely to disrupt hydrophobic interactions and separate loosely associated proteins. In both types of detergent extracts, a prominent protein band corresponding to AKAP15 was present in anti-$Ca_V1.2$ immunoprecipitates that were analyzed by SDS-PAGE and immunoblotting with anti-AKAP15 antibody (Fig. 1*B*). In contrast, no co-immunoprecipitation of AKAP15 was observed when nonimmune rabbit IgG was used in control immunoprecipitations under identical conditions (Fig. 1*B*). As previously

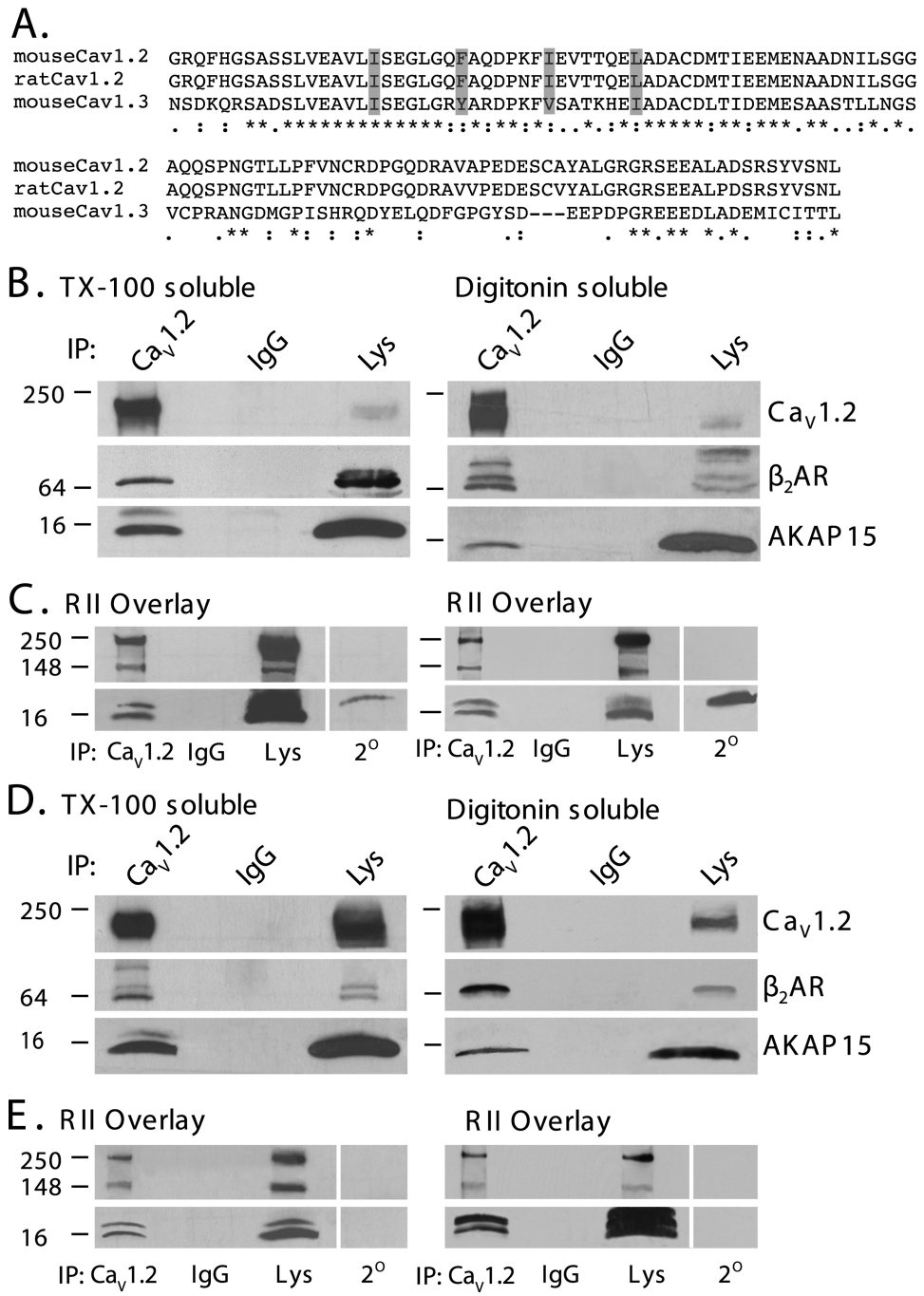

FIGURE 1. **Co-immunoprecipitation of AKAP15 with $Ca_V1.2$ channels.** *A*, amino acid sequence alignment of the LZ-like region identified in the distal C-terminal domain of $Ca_V1.2$ channels that interacts with AKAP15 in other members of the Ca_V1 family. *B*, proteins were immunoprecipitated (*IP*) from membrane extracts of adult mouse brain with an anti-$Ca_V1.2$ antibody (*first lane*) or control IgG (*second lane*) as indicated. Immunoblots were probed with anti-$Ca_V1.2$ (*upper*), anti-β_2AR (*middle*), or anti-AKAP15 (*lower*). Positive control for immunoblotting was 40 μl of brain extract (*third lane*). *TX-100*, Triton X-100. *C*, immunoblots were stripped and reprobed with RII-biotin to reveal all AKAPs: anti-$Ca_V1.2$ (*first lane*), control IgG (*second lane*), 40 μl of brain extract (*third lane*), or secondary antibody alone (*fourth lane*). *D*, proteins were immunoprecipitated from E18 brain extracts with anti-$Ca_V1.2$ antibody (*first lane*) or control IgG (*second lane*) and brain lysate (*third lane*). Immunoblots were then probed with anti-$Ca_V1.2$ (*upper*), anti-β_2AR (*middle*), and anti-AKAP15 (*lower*). *E*, proteins were immunoprecipitated from E18 brain extracts with anti-$Ca_V1.2$ (*first lane*) or control IgG (*second lane*) and AKAPs were detected using the RII-biotin assay. Brain lysate (40 μl) (*third lane*) served as a positive control, and secondary antibody alone (*fourth lane*) served as a negative control for the RII overlay.

reported (38), β_2ARs were also specifically co-immunoprecipitated with $Ca_V1.2$ channels (Fig. 1*B*).

To detect other AKAPs associated with specifically immunoprecipitated $Ca_V1.2$ channels, we re-probed immunoblots using the RII-biotin overlay assay to detect all AKAPs (25). As shown in Fig. 1*C* (*first lane*), three AKAPs with molecular masses corresponding to MAP2B (280 kDa), AKAP150 (150 kDa), and AKAP15 (15 kDa) were co-immunoprecipitated with $Ca_V1.2$ channels from brain membranes, but no co-immunoprecipitation was observed with non-immune IgG (Fig. 1*C*, *second lane*) or with secondary antibody alone (Fig. 1*C*, *fourth lane*). Although we observed Yotiao, another abundant neuro-

nal AKAP, in our lysates, we did not find that it co-immunoprecipitated with $Ca_V1.2$ channels, further verifying the specificity of this interaction. These results confirm the identification of AKAP15 in these co-immunoprecipitates as well as β_2ARs, MAP2B, and AKAP150 as reported previously (28, 39). We have previously found that AKAP15 binds directly to cardiac $Ca_V1.2$ channels via the C-terminal LZ motif (24), so it is likely that the co-immunoprecipitation observed here reflects direct interaction between these two proteins. On the other hand, it is possible that β_2ARs, MAP2B, and AKAP150 are indirectly associated with $Ca_V1.2$ channels through intermediary proteins.

Co-immunoprecipitation of $Ca_V1.2$ Channels and AKAP15 from Embryonic Mouse Brain—Having established that AKAP15 associates with $Ca_V1.2$ channels in adult brain, we tested whether AKAP15 also associates with $Ca_V1.2$ channels earlier in development. Similar to adults, AKAP15 co-immunoprecipitated with $Ca_V1.2$ channels from embryonic day 18 (E18) brain with either Triton X-100 or digitonin as detergent (Fig. 1*D*). MAP2B, AKAP150, and the β_2AR were also co-immunoprecipitated at this time point (Fig. 1, *D* and *E*), indicating that $Ca_V1.2$ channel/PKA signaling complexes are formed by E18. AKAP15 and the other associated proteins were not observed in immunoprecipitates obtained with control IgG (Fig. 1, *D* and *E*, *second lanes*), and there was no staining with secondary antibody alone in the RII-biotin overlay assay (Fig. 1*E*, *fourth lane*), confirming the specificity of immunoblotting.

Comparison of the average levels of co-immunoprecipitation of AKAP150, MAP2B, and AKAP15 detected in the RII-biotin overlay assay revealed that MAP2B and AKAP15 had similar levels of association with $Ca_V1.2$ channels in E18 mouse brain, whereas higher levels of AKAP15 were observed in association with $Ca_V1.2$ channels in adult brain than AKAP150 or MAP2B (supplemental Fig. 1, *A–D*).

Localization of $Ca_V1.2$ Channels, AKAP15, MAP2B, and β_2ARs in Brain Neurons—Previous studies from our laboratory have established that AKAP15 and $Ca_V1.2$ channels are precisely co-localized in skeletal and cardiac myocytes (24, 26). L-type calcium currents have different functional roles in the dendrites and cell bodies of neurons; therefore, it is of interest to determine which subcellular compartments have $Ca_V1.2$ channels co-localized with AKAP15 and which classes of neurons contain this signaling complex. To determine the subcellular distribution of AKAP15 relative to neuronal $Ca_V1.2$ channels *in vivo*, we performed double-label immunocytochemistry on adult mouse brain slices using chicken anti-$Ca_V1.2$ and rabbit anti-AKAP15 antibodies. Sagittal tissue sections labeled with polyclonal antibodies against $Ca_V1.2$ channels (*green*, Fig. 2, *B*, *E*, and *H*) revealed staining concentrated in the soma and proximal dendrites, as expected from previous work (20, 21). AKAP15 showed a similar distribution (*red*, Fig. 2, *A*, *D*, and *G*). Overlapping localization of these proteins was evident in both dorsal cerebral cortex and the CA1/3 region of the hippocampus (*yellow*, Fig. 2, *C*, *F*, and *I*) when the images of their individual staining patterns were merged.

MAP2B is a 280-kDa AKAP that was previously found to be associated with $Ca_V1.2$ channels (Ref. 28 and Fig. 1). To compare the localization of MAP2B and AKAP15, sagittal sections of adult mouse brain and cultured neurons were examined

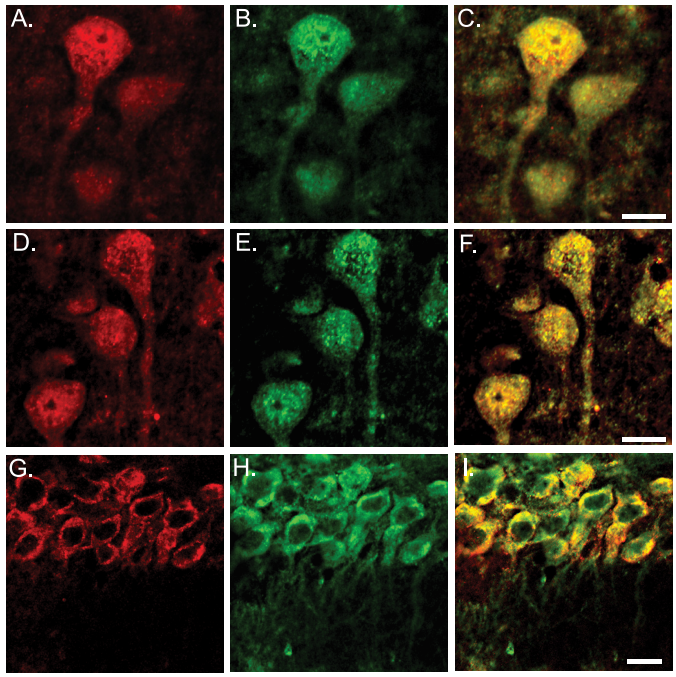

FIGURE 2. **Localization of AKAP15 and $Ca_V1.2$ channels in cortical and hippocampal neurons.** Sections of adult mouse brain were cut, fixed, and double-labeled with antibodies against $Ca_V1.2$ and AKAP15 as described under "Materials and Methods." Representative examples of slices double-labeled with antibodies specific for AKAP15 or $Ca_V1.2$ channels are shown. *A*, *D*, and *G*, AKAP15, *red*. *B*, *E*, and *H*, $Ca_V1.2$, *green*. *C*, *F*, and *I*, merged images reveal double-labeled structures in *yellow*. *A–F*, dorsal cortex; *G–I*, hippocampal CA1 neurons. *Scale bars* = 20 μm.

using double-labeling and confocal immunofluorescence microscopy. MAP2B was primarily localized to proximal and distal dendrites with little cell body staining (*red*, Fig. 3, *B* and *E*), whereas $Ca_V1.2$ channels were concentrated in the cell body and proximal dendrites (*green*, Fig. 3, *A* and *D*). Thus, the distributions of AKAP15 and MAP2B are partially complementary, with more MAP2B immunostaining in the distal dendrites and more AKAP15 in the cell bodies and proximal dendrites of these neurons (Fig. 3, *C* and *F*). In neurons cultured for 14 days *in vitro*, MAP2B was more strongly localized to dendrites (*red*, Fig. 3, *H* and *K*) compared with AKAP15, which showed stronger localization in the soma and proximal dendrites (*blue*, Fig. 3*J*). Quantification of AKAP15 localization showed that the ratio of AKAP15 staining intensity in the cell body is 3.5-fold greater than MAP2B (Fig. 3*L*). The partially complementary distribution of these two AKAPs suggests that they have distinct localizations and different functional roles in neurons.

Association of $Ca_V1.3$ Channels with AKAP15, MAP2B, and β_2ARs—Alignment of the C-terminal domains of $Ca_V1.2$ and $Ca_V1.3$ channels (Fig. 1*A*) shows striking conservation of the amino acid sequence of $Ca_V1.3$ channels in the heptad repeat of hydrophobic residues that binds AKAP15 via a modified LZ. Sequence comparison of the adjacent regulatory domains in $Ca_V1.3$ channels, including the proximal C-terminal regulatory domain, the proteolytic cleavage site, and the distal C-terminal regulatory domain, also shows strongly conserved amino acid sequence at these sites (41). To examine the interactions between $Ca_V1.3$ channels and other members of the Ca_V1 channel signaling complex, we tested whether AKAP15, MAP2B, and β_2AR are

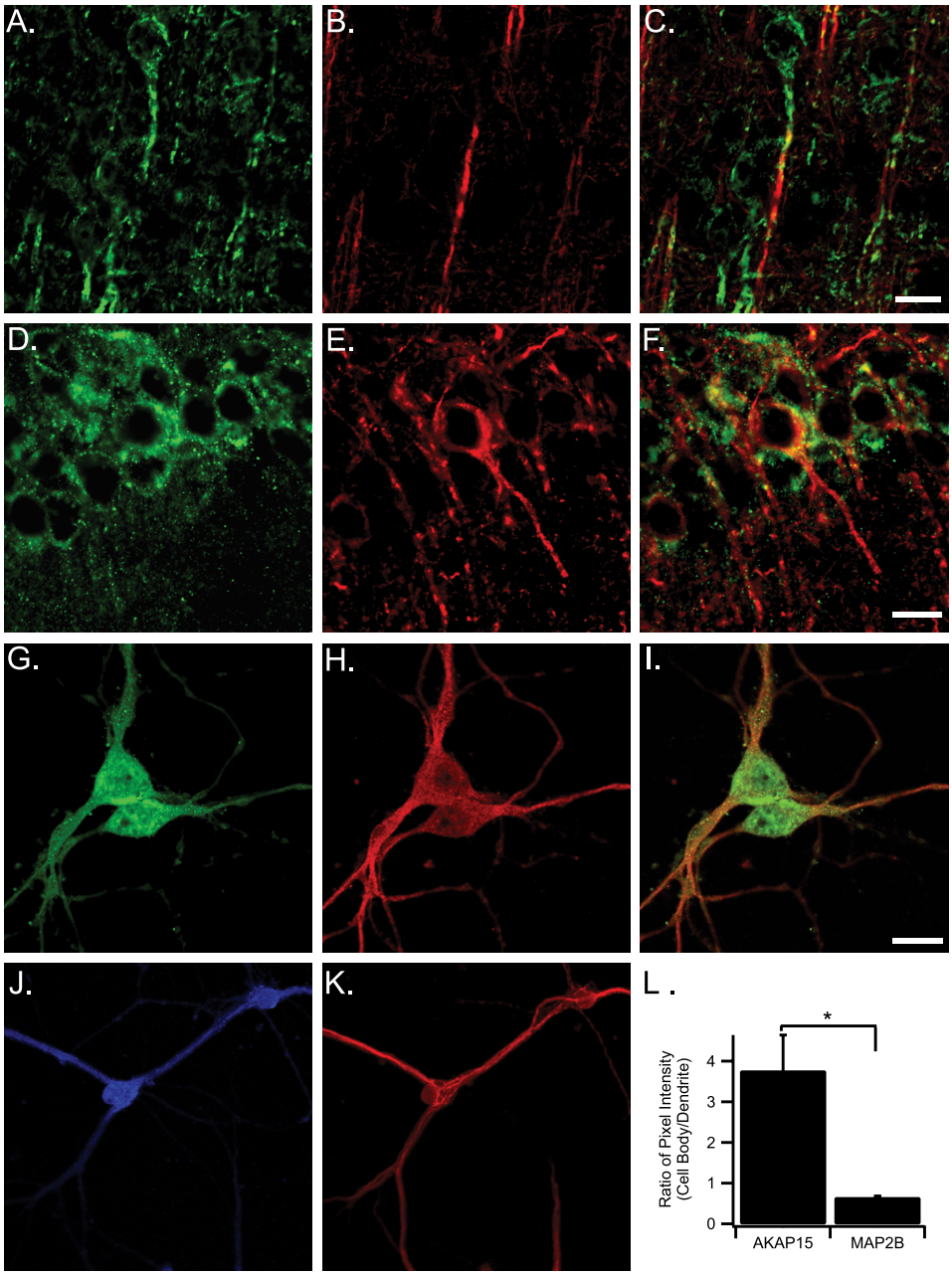

FIGURE 3. **Localization of $Ca_V1.2$ channels and MAP2B in cortical and hippocampal neurons.** Sections of adult mouse brain were cut, fixed, and double-labeled with antibodies against $Ca_V1.2$ and MAP2B as described under "Materials and Methods." *A* and *D*, $Ca_V1.2$, *green*. *B* and *E*, MAP2B, *red*. *C* and *F*, merged images. Regions of overlap are shown in *yellow*. *A–C*, dorsal cerebral cortex; *D–F*, CA3 hippocampus *G*, *H*, and *I*, cultured hippocampal neurons were fixed and double-labeled with anti-$Ca_V1.2$ (*G*) and anti-MAP2B (*H*). Regions of overlap are shown in *yellow*. *J* and *K*, representative examples of cultured hippocampal neurons that were fixed and double-labeled with anti-AKAP15 (*J*) and anti-MAP2B (*K*) are shown. *L*, quantification of localization of neuronal AKAPs in the cell body and dendritic regions are shown. Staining intensity of MAP2B and AKAP15 were quantified by determining mean pixel density for regions of interest in the dendrites and cell body. The ratios of the cell body pixel intensities to the dendritic pixel intensities were determined for each cell and antibody, and the ratios were averaged for each antibody. *Asterisk*, $p < 0.01$, Student's *t*-test. *Scale bars* = 40 μm.

associated with $Ca_V1.3$ channels. Immunoprecipitation with a $Ca_V1.3$-specific antibody and subsequent immunoblotting for AKAP15 and the β_2AR revealed that they both co-immunoprecipitated with $Ca_V1.3$ channels after both Triton X-100 solubilization (Fig. 4*A*, *first lane*) and digitonin solubilization (data not shown). Re-probing the immunoblots using the RII-biotin overlay assay revealed protein bands consistent in size with MAP2B and AKAP15 (Fig. 4*B*, *first lane*). No staining was observed with control nonimmune IgG (Fig. 4, *A* and *B*, *second lanes*) or with secondary antibody alone (Fig. 4*B*, *fourth lane*), confirming the specificity of antibody staining. Comparison of co-immunoprecipitation of AKAP15, AKAP150, and MAP2B in parallel experiments using the RII-biotin overlay assay revealed that they are associated with $Ca_V1.2$ and $Ca_V1.3$ channels at similar levels in adult mouse brain, with increased levels of AKAP15 compared with MAP2B and AKAP150 in both cases (supplemental Fig. 1*D*).

Localization of $Ca_V1.3$ Channels, AKAP15, MAP2B, and β_2AR—Previous results have shown that $Ca_V1.3$ channels are located in cell bodies and proximal dendrites of hippocampal and cortical neurons (20). As the $Ca_V1.3$ channel comprises

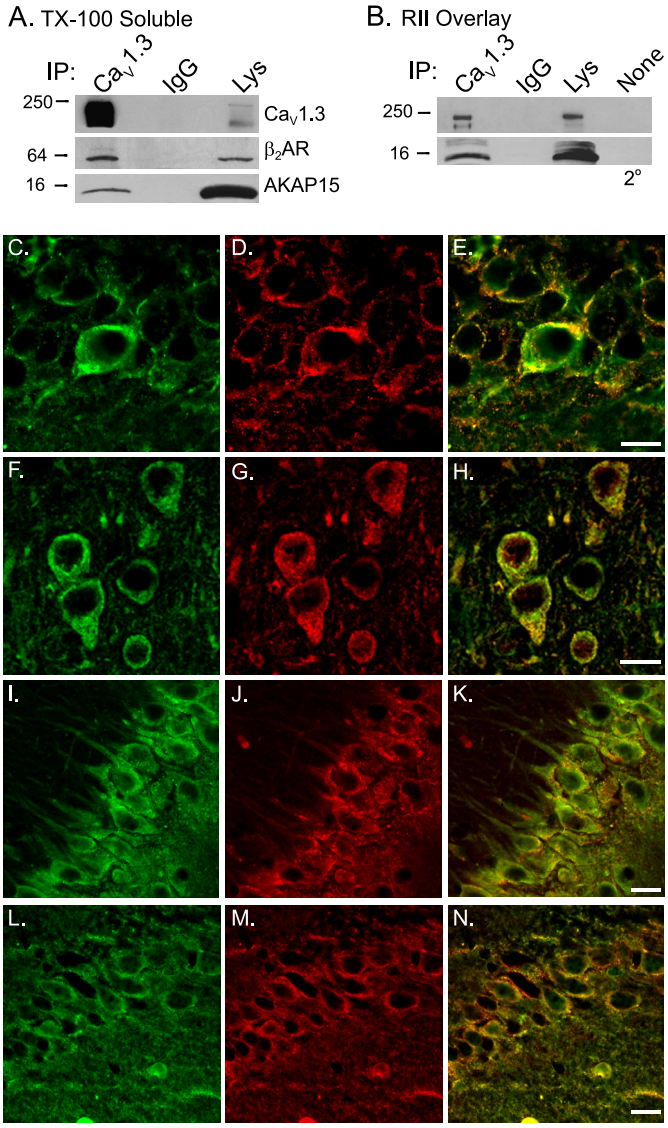

FIGURE 4. **Coimmunoprecipitation and localization of $Ca_V1.3$ channels and AKAP15.** *A*, isolated mouse brain membrane proteins were extracted with Triton X-100 (*TX-100*), and proteins were immunoprecipitated (*IP*) with anti-$Ca_V1.3$ antibody (*first lane*) or control IgG (*second lane*). Immunoblots were probed with anti-$Ca_V1.3$ (*upper*), anti-β_2AR (*middle*), or anti-AKAP15 (*lower*). The positive control for immunoblotting was 40 μl of brain extract (*third lane*). *B*, immunoblots from *panel A* were stripped and reprobed with RII-biotin to reveal AKAPs co-immunoprecipitated with $Ca_V1.3$ channels (*first lane*). *C–N*, representative examples are shown of mouse brain slices double-labeled with antibodies specific for AKAP15 (*green*, *panels C*, *F*, *I*, and *L*), $Ca_V1.3$ (*red*, *panels D*, *G*, *J*, and *M*), and merged images (*yellow*, *panels E*, *H*, *K*, and *N*). *C–H*, dorsal cortex. *I–K*, hippocampal CA3. *L–N*, hippocampal CA1.

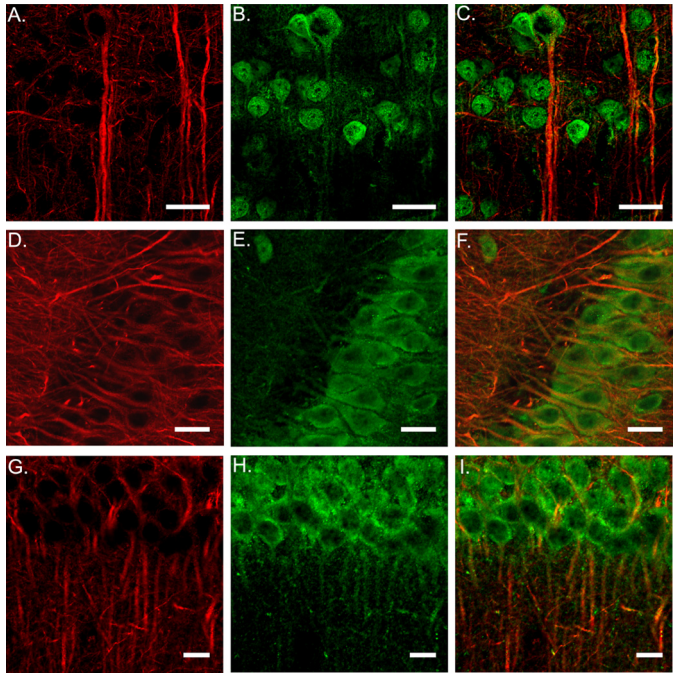

FIGURE 5. **Localization of MAP2B and $Ca_V1.3$ channels in cortical and hippocampal neurons.** Sections of adult mouse brain were cut, fixed, and double-labeled with antibodies against $Ca_V1.3$ and MAP2B as described under "Materials and Methods." Representative examples of slices double-labeled with antibodies specific for $Ca_V1.3$ channels and MAP2B are illustrated. *A–C*, dorsal cerebral cortex; *D–F*, hippocampal CA3 region; *G–I*, hippocampal CA1 region. *A*, *D*, and *G*, Map2B, *red*; *B*, *E*, and *H*, $Ca_V1.3$, *green*; *C*, *D*, and *I*, merged images. Areas of overlap are *yellow*. *Scale bars* are 50 μm.

about 22% of neuronal Ca_V1 channels (20), we would expect $Ca_V1.3$ channels to only partially co-localize with AKAP15 and other members of the channel complex. We examined the distribution of $Ca_V1.3$ channels and AKAP15 using double immunostaining in mouse sagittal brain sections. Dense labeling of $Ca_V1.3$ channels was observed in cell bodies and proximal dendrites in all regions of the dorsal cerebral cortex and hippocampus (*green*, Fig. 4, *C*, *F*, *I*, and L), with similar staining patterns as AKAP15 (*red*, Fig. 4, *D*, *G*, *J*, and *M*). Regions of overlapping immunostaining are observed in *yellow* when images of their respective staining patterns are merged (*yellow*, Fig. 4, *E*, *H*, *K*, and *N*). Immunocytochemical studies showed that β_2AR and $Ca_V1.3$ channels also have an overlapping distribution in cortical and hippocampal neurons (supplemental Fig. 2), as expected from our co-immunoprecipitation studies showing their specific interaction. In contrast to the localization of AKAP15, examination of MAP2B shows staining in proximal and distal dendrites in adult dorsal cortex (*red*, Fig. 5*A*) and CA1/CA3 regions (*red*, Fig. 5, *D* and *G*). Antibodies against $Ca_V1.3$ channels give a smooth pattern of staining in cell bodies and proximal dendrites (*green*, Fig. 5, *B*, *E*, and *H*). Merged images show primarily distinct localizations of MAP2B and $Ca_V1.3$ channels, except for small areas of overlap in the proximal dendrites and in some regions along the distal dendrites (*yellow*, Fig. 5, *C*, *F*, and *I*). Together with the images of Fig. 4, these results indicate that AKAP15 and MAP2B have complementary localizations, with MAP2B more concentrated in distal dendrites and AKAP15 more concentrated in cell bodies and proximal dendrites. The localization of $Ca_V1.3$ channels overlaps more completely with AKAP15 (Fig. 4) than with MAP2B (Fig. 5). Therefore, our results suggest that $Ca_V1.3$ channels form complexes with AKAP15 in their cell bodies and proximal dendrites as well as less extensive complexes with MAP2B in their distal dendrites. These localizations may differ in neurons in other regions of the brain.

Disruption of the Distal C Terminus of $Ca_V1.2$ Channels—Similar to the α_1 subunit of skeletal muscle $Ca_V1.1$ channels, the $Ca_V1.2$ channel exists in two size forms, a full-length form and a distal C-terminal truncated form resulting from post-translational proteolytic processing *in vivo* (20, 31). AKAP15 binds to the distal C terminus and is required for regulation of

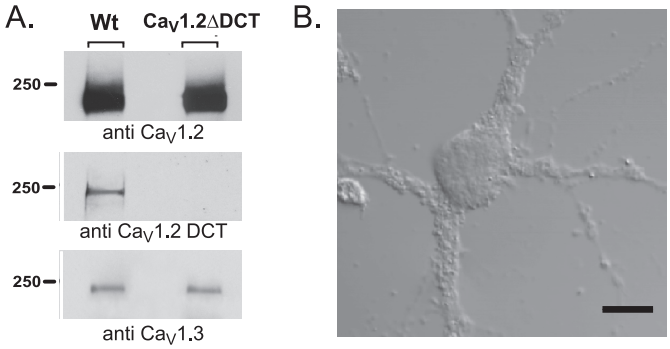

FIGURE 6. **Generation of $Ca_V1.2\Delta DCT$ mice.** *A*, brain calcium channel expression in $Ca_V1.2\Delta DCT$ mice. Brain membrane proteins (100 μg) from wild-type and homozygous mice at E18 were analyzed by SDS-PAGE and immunoblotting. *Top*, anti-$Ca_V1.2$ against the intracellular loop between domains I and II of $Ca_V1.2$ channels is shown. *Middle*, anti-CH2 against the distal C-terminal tail of $Ca_V1.2$ is shown. *Bottom*, anti-$Ca_V1.3$. *B*, a representative bright-field view of a hippocampal pyramidal neuron dissociated from E18 mice. The pyramidal neurons were identified by bulbous, triangular cell bodies with prominent proximal dendritic extensions. *Scale bar* = 25 μm.

$Ca_V1.2$ channels in cardiac myocytes by PKA (24, 37). These studies of cardiac myocytes imply that the C terminus exerts an inhibitory effect on L-type calcium currents conducted by Ca_V1 channels, but the effects of C-terminal truncation have not been investigated in neurons. To examine the effects of C-terminal truncation *in vivo*, we generated a targeted knock-in mouse line with a stop codon that deletes the distal C terminus from the protein at Gly-1796 ($Ca_V1.2\Delta DCT$ (33)). Although the $Ca_V1.2\Delta DCT$ heterozygous mutant mice show development, lifespan, and gross phenotype that are similar to their wild-type littermates, matings of heterozygotes consistently failed to generate viable homozygous mutant offspring when the genotypes were analyzed upon weaning. Approximately Mendelian ratios of the three genotypes were obtained in 7 litters recovered at E16–18: 16 wild types, 25 heterozygotes, and 15 homozygotes. The homozygous mutant pups were indistinguishable from the wild-type littermates at E16–18, but they die perinatally from vascular dysfunction, which also leads to dilated cardiac myopathy and heart failure (33).

When probed with the anti-$Ca_V1.2$ antibody that recognizes an epitope in the intracellular loop connecting domains II and III, membranes from E18 wild-type and $Ca_V1.2\Delta DCT$ mice had similar amounts of $Ca_V1.2$ channels (Fig. 6*A*, *top*). In contrast, immunoblots using an antibody against the truncated distal C terminus detect $Ca_V1.2$ channels in wild-type but not in homozygous $Ca_V1.2\Delta DCT$ mice, confirming successful truncation of distal C-terminal domain in $Ca_V1.2$ channels (Fig. 6*A*, *middle*). There was no apparent up-regulation of $Ca_V1.3$ channels in homozygous mutant mice (Fig. 6*A*, *bottom*). Neurons dissociated from $Ca_V1.2\Delta DCT$ homozygotes at E18 (Fig. 6*B*) thrived in subsequent cell culture and could be studied by immunocytochemical, physiological, and biochemical methods.

Localization of Ca_V1 Channels in Neurons of $Ca_V1.2\Delta DCT$ Mice—As in neurons in adult hippocampus and cerebral cortex, $Ca_V1.2$ channels were localized to the cell bodies and proximal dendrites of cultured wild-type (Fig. 7, *A* and *B*) and $Ca_V1.2\Delta DCT$ (Fig. 7, *C* and *D*) hippocampal neurons. Similarly, $Ca_V1.3$ channels were localized in higher density in the cell

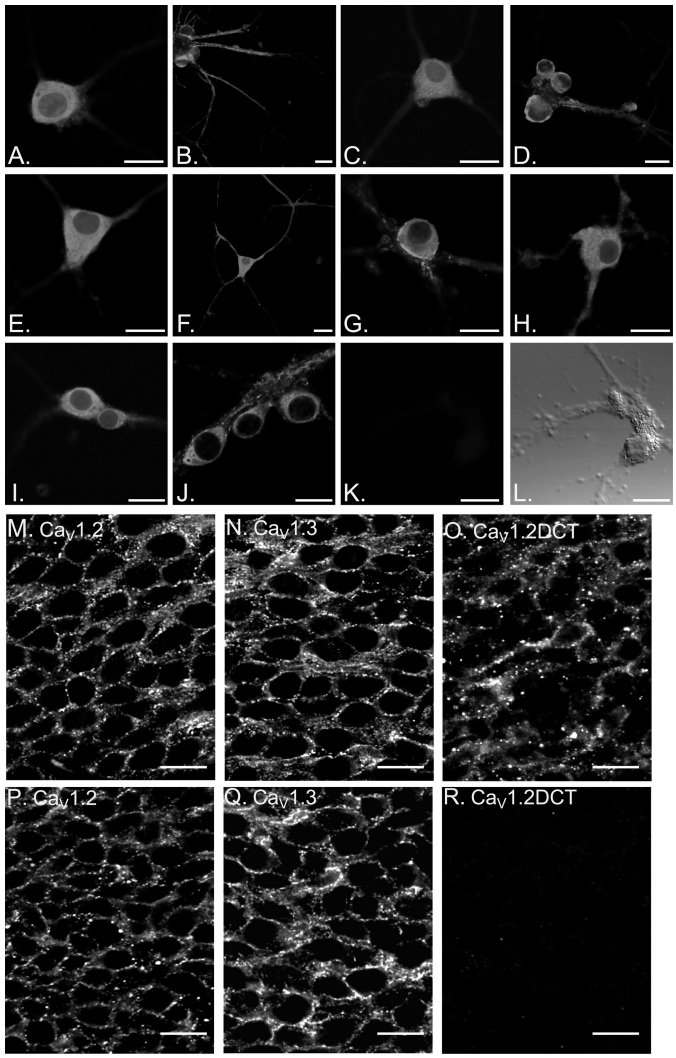

FIGURE 7. **Localization of Ca_V1 channel complexes in the dorsal cortex of $Ca_V1.2\Delta DCT$ mice.** *A–D*, $Ca_V1.2$ staining along the cell body and dendrites of cultured hippocampal neurons from wild-type (*A* and *B*) and $Ca_V1.2\Delta DCT$ mice (*C* and *D*). *E–H*, $Ca_V1.3$ staining of cultured hippocampal neurons from wild-type (*E* and *F*) and $Ca_V1.2\Delta DCT$ mice (*G* and *H*). *I–K*, cultured hippocampal neurons stained with anti-CH2 recognizing the distal C terminus of $Ca_V1.2$. *I* and *J*, wild-type hippocampal neurons. *K*, $Ca_V1.2\Delta DCT$ neuron. *L*, same neuron as *I* is viewed using transmitted light and Nomarski optics. *M* and *O*, wild-type mouse brain slices stained with anti-$Ca_V1.2$ (*M*) anti-$Ca_V1.3$ (*N*) or anti-CH2 (*O*). *P* and *R*, $Ca_V1.2\Delta DCT$ mouse brain slices stained with anti-$Ca_V1.2$ (*P*) anti-$Ca_V1.3$ (*Q*) or anti-CH2 (*R*). *Scale bars* = 40 μm.

bodies of cultured neurons from both wild-type (Fig. 7, *E* and *F*) and $Ca_V1.2\Delta DCT$ (Fig. 7, *G* and *H*) mice. Anti-CH2 antibody, recognizing the $Ca_V1.2$ distal C terminus, stained wild-type (Fig. 7, *I* and *J*) but not $Ca_V1.2\Delta DCT$ neurons (Fig. 7, *K* and *L*). Examination of the localization of calcium channels in brain slices from the developing cerebral cortex of E18 mice by immunocytochemistry and confocal microscopy revealed similar staining of the cell surface of neurons for wild-type (Fig. 7*M*) and $Ca_V1.2\Delta DCT$ mice (Fig. 7*P*), and no apparent compensatory changes in localization of $Ca_V1.3$ channels were evident (Fig. 7, *N* and *Q*). $Ca_V1.2\Delta DCT$ animals lack immunostaining with antibodies against the $Ca_V1.2$ distal C terminus as expected (Fig. 7*R*).

Localization of AKAP15 in Neurons of $Ca_V1.2\Delta DCT$ Mice—In skeletal and cardiac myocytes, $Ca_V1.2$ channels bind

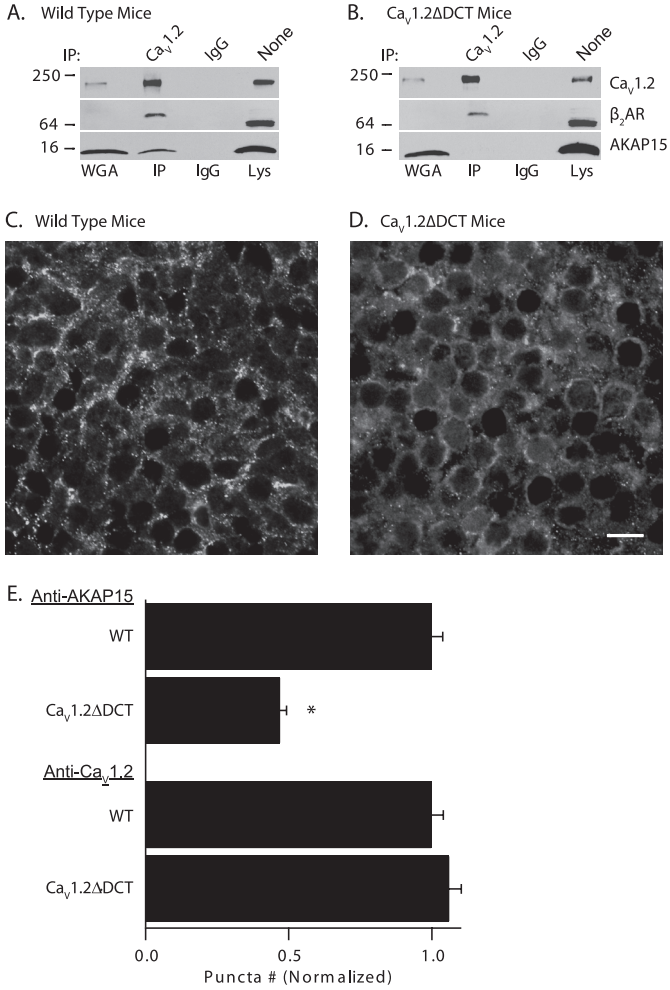

FIGURE 8. **Association of AKAP15 with the distal C terminus of $Ca_V1.2$ channels in wild-type and $Ca_V1.2\Delta DCT$ mice.** *A* and *B*, calcium channels from wild-type (*A*) and $Ca_V1.2\Delta DCT$ (*B*) mice were solubilized, and calcium channel complexes were immunoprecipitated with antibodies against $Ca_V1.2$ channels. Immunoprecipitates (*IP*) and lysate (*Lys*) were analyzed by SDS-PAGE and immunoblotting with antibodies against $Ca_V1.2$, AKAP15, and β_2AR. Brain membrane lysate, enriched by affinity chromatography on a wheat germ agglutinin column (*WGA*) was used as a positive control for immunoblotting. *C* and *D*, immunolocalization of AKAP15 in slices of the dorsal cerebral cortex from wild-type (*C*) and $Ca_V1.2\Delta DCT$ (*D*) mice. *Scale bar* = 40 μm. *E*, quantification of anti-AKAP15 puncta in wild-type and $Ca_V1.2\Delta DCT$ mice is shown. The number of puncta was counted in regions of interest of equal size in each section. Counts for $Ca_V1.2\Delta DCT$ sections were normalized to the mean of the wild-type sections for each experiment and each antibody. The mean normalized counts are plotted. $Ca_V1.2$, $n = 3$ experiments; AKAP15, $n = 4$ experiments. 2–4 slices were counted per experiment. *Asterisk*, $p < 0.01$, Student's *t* test.

AKAP15 at a specific site in the distal C-terminal domain, beyond the point of truncation of $Ca_V1.2\Delta DCT$ (24, 37). To test whether AKAP15 interacts with $Ca_V1.2$ channels via the distal C terminus *in vivo*, $Ca_V1.2$ channels in brain membrane lysates of E18 wild-type or $Ca_V1.2\Delta DCT$ mice were immunoprecipitated with an anti-$Ca_V1.2$ antibody or control IgG and analyzed by SDS-PAGE and immunoblotting for association of $Ca_V1.2$ with AKAP15 and β_2ARs (Fig. 8, *A* and *B*). Immunoblotting revealed an AKAP15 band at an apparent molecular mass of 15 kDa co-immunoprecipitated with $Ca_V1.2$ channels from wild-type mice, but this protein band was completely absent from $Ca_V1.2\Delta DCT$ mice (Fig. 8, *A* and *B*, *second lanes*). In contrast, co-immunoprecipitation of the β_2AR was not reduced by deletion of the distal C terminus, supporting the idea it does not bind primarily to the distal C-terminal region of $Ca_V1.2$ channels (Fig. 8, *A* and *B*, *second lanes*).

Deletion of the distal C-terminal domain of $Ca_V1.2$ channels would be expected to alter the co-localization of the bound AKAP15 with $Ca_V1.2$ channels in $Ca_V1.2\Delta DCT$ mice. Sections of developing cerebral cortex at E18 were examined for AKAP15 immunostaining, and these images revealed a significant change in distribution of AKAP15 on the cell surface from a punctate pattern to a smoother pattern in $Ca_V1.2\Delta DCT$ mice (Fig. 8, *C* and *D*). Quantification of AKAP15 puncta revealed a 53 ± 0.1% reduction in $Ca_V1.2\Delta DCT$ mice (Fig. 8*E*, $n = 4$ experiments, $p < 0.01$). These results show that AKAP15 localization is dependent on the intact distal C terminus of $Ca_V1.2$ channels and suggest that AKAP15 can no longer bind to the distal C-terminal domain of $Ca_V1.2$ channels in punctate clusters because its binding site has been deleted.

Functional Properties of Calcium Channels in $Ca_V1.2\Delta DCT$ Neurons—When expressed in heterologous cells such as *Xenopus* oocytes and human embryonic kidney cells, truncated $Ca_V1.2$ channels are more active than wild type (42–44). To examine the physiological significance of the distal C terminus in the function and regulation of $Ca_V1.2$ channels *in vivo*, we dissociated neurons from mouse hippocampus at E18 and measured whole-cell L-type barium currents through Ca_V1 channels in wild-type and $Ca_V1.2\Delta DCT$ neurons. Hippocampal pyramidal cells were identified by their bulbous, triangular cell bodies with prominent proximal dendritic extensions (Fig. 6*B*). After establishing the whole-cell patch clamp configuration and recording stable currents in 5 mM Ba^{2+}, we inhibited L-type barium currents by perfusing the L-type calcium channel blocker nimodipine (10 μM) (Fig. 9*A*). We calculated nimodipine-sensitive L-type barium current by subtracting the barium current in the presence of nimodipine from total current. Contrary to our expectations from experiments with transfected cells, there was a substantial decrease in the L-type barium current in neurons from heterozygous and homozygous $Ca_V1.2\Delta DCT$ neurons (Fig. 9*B*). Wild-type, heterozygous, and homozygous $Ca_V1.2\Delta DCT$ pyramidal neurons conducted similar non-L-type barium currents (Fig. 9*C*). Despite the large change in current amplitude, no significant changes in the voltage dependence of activation of L-type barium currents were observed across the three genotypes (Fig. 9*B*). These results reveal a previously unrecognized requirement for the distal C-terminal domain in maintaining normal functional expression of $Ca_V1.2$ channels in neurons *in vivo*.

Regulation of CREB Phosphorylation in Neurons from $Ca_V1.2\Delta DCT$ Mice—It is well established that gene expression and new protein synthesis are required for long-lasting changes of synaptic strength, but it is not known what signaling mechanisms transmit information from the membrane to the nucleus to support gene expression. The transcription factor CREB has been shown to drive the expression of a number of genes that regulate neuronal survival and plasticity, and phosphorylation of CREB on Ser^{133} is thought to be an important process underlying long-term memory (9–13, 45–47). Calcium entering through neuronal Ca_V1 channels has a privileged role in signaling to activation of CREB phosphorylation (7, 8). More-

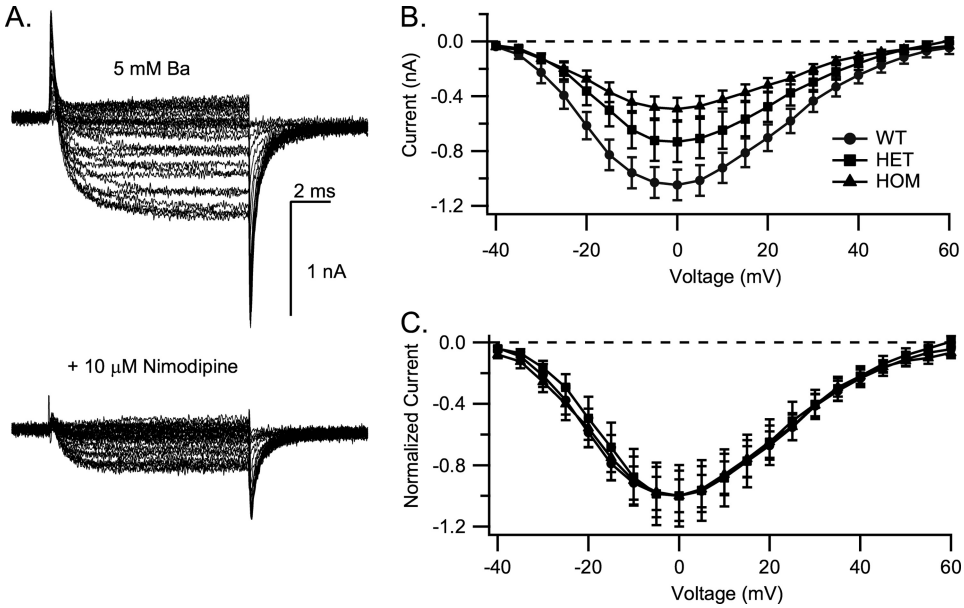

FIGURE 9. **Effects of C-terminal truncation on the functional properties of $Ca_V1.2$ channels in cultured hippocampal neurons.** Inward barium currents (I_{Ba}) were recorded from CA1/3 hippocampal pyramidal cells cultured for 8–14 days from wild-type, heterozygous, or homozygous $Ca_V1.2\Delta DCT$ mice. *A*, representative families of barium currents evoked by depolarizations ranging from −60 to 100 mV in 10-mV steps from a holding potential of −70 mV under control conditions (*top*), and after perfusion of 10 μM nimodipine (*bottom*). *B*, mean current-voltage curves for nimodipine-sensitive barium current (L-type) are shown. *HET*, heterozygous; *HOM*, homozygous. *C*, mean current-voltage curves are shown for barium current after subtraction of traces recorded in the presence of 10 μM nimodipine to yield nimodipine-insensitive barium current.

over, experiments in cultured neurons suggest that the C-terminal domain of the L-type calcium channel directly regulates CREB phosphorylation in the nucleus (8).

To determine whether the distal C-terminal domain of $Ca_V1.2$ channels containing the AKAP15 interaction site is required for activation of CREB phosphorylation, we cultured hippocampal neurons from E18 wild-type and $Ca_V1.2\Delta DCT$ mice for 10–14 days *in vitro*. We depolarized these neurons with 65 mM KCl after blocking *N*-methyl-D-aspartate receptors with D,L-,-2-amino-5-phosphonovaleric acid, α-amino-3-hydroxy-5-methyl-4-isoxazolepropionic acid (AMPA) receptors with 6-cyano-7-nitroquinoxaline-2,3-dione (CNQX), and sodium channels with tetrodotoxin, and we measured CREB Ser^{133} phosphorylation in response to depolarization and calcium entry. Neurons were lysed in boiling sample buffer, proteins were separated by SDS-PAGE, and the level of phospho-CREB was measured and compared with total CREB by immunoblotting with normalization to actin controls (Fig. 10, *A–D*). As a positive control treatment, we tested the effect of brain-derived neurotrophic factor, which increases both CREB and ERK phosphorylation (48, 49). As expected, brain-derived neurotrophic factor increased both phospho-CREB and phospho-ERK in wild-type animals (Fig. 10*A*). Quantification of the results for brain-derived neurotrophic factor stimulation of phospho-CREB showed that it was increased by 2.23 ± 0.27-fold (Fig. 10*E*). Stimulation with 65 mM KCl also gave a substantial increase of both phospho-CREB (Fig. 10, *A* and *E*) and phospho-ERK (Fig. 10*C*). Quantification of these results revealed that KCl stimulation increased pCREB by 1.96 ± 0.17-fold in hippocampal cultures from wild-type mice ($p < 0.001$, Fig. 10*E*), but this effect was reduced to 1.45 ± 0.14 ($p < 0.02$) in heterozygous $Ca_V1.2\Delta DCT$ mice and was reduced to the unstimulated base line in homozygous $Ca_V1.2\Delta DCT$ mice (1.14 ± 0.10, $p > 0.2$, Fig. 10*E*).

Finally, we examined whether KCl-stimulated depolarization of Ca_V1 channels would reveal similar loss of excitation-phosphorylation coupling using confocal microscopy with antibodies against CREB and pCREB. KCl depolarization increased phosphorylation of CREB in the nucleus of wild-type neurons (Fig. 10, *G* and *L*) but not in $Ca_V1.2\Delta DCT$ neurons (Fig. 10, *J* and *L*). Unstimulated phosphorylation of CREB in the nucleus appears similar in both wild-type and $Ca_V1.2c\Delta DCT$ neurons (Fig. 10, *F*, *I*, and *L*), and total CREB does not appear to change (Fig. 10, *H*, *K*, and *L*). These results confirm our conclusions as seen in our immunoblotting experiments that neurons from $Ca_V1.2\Delta DCT$ mice have impaired coupling of depolarization to phosphorylation of CREB.

DISCUSSION

Our results reveal three previously unrecognized functional roles for the distal C-terminal domain in the signaling complexes formed by Ca_V1 channels and AKAPs. First, in contrast to previous studies (28), the distal C-terminal domain of $Ca_V1.2$ channels binds AKAP15 and alters its localization in neurons *in vivo*. $Ca_V1.3$ channels also form a signaling complex with AKAP15 in brain neurons. Second, against expectations from previous studies in transfected cells (42–44), the distal C-terminal domain is required for normal levels of functional expression of $Ca_V1.2$ channels in neurons *in vivo*. Finally, in contrast to expectations from previous work showing that binding of calmodulin to the IQ-like motif in the proximal C-terminal domain is required for excitation-transcription coupling (8), we find the distal C-terminal domain of $Ca_V1.2$ channels is also required for normal coupling of excitation to phosphorylation

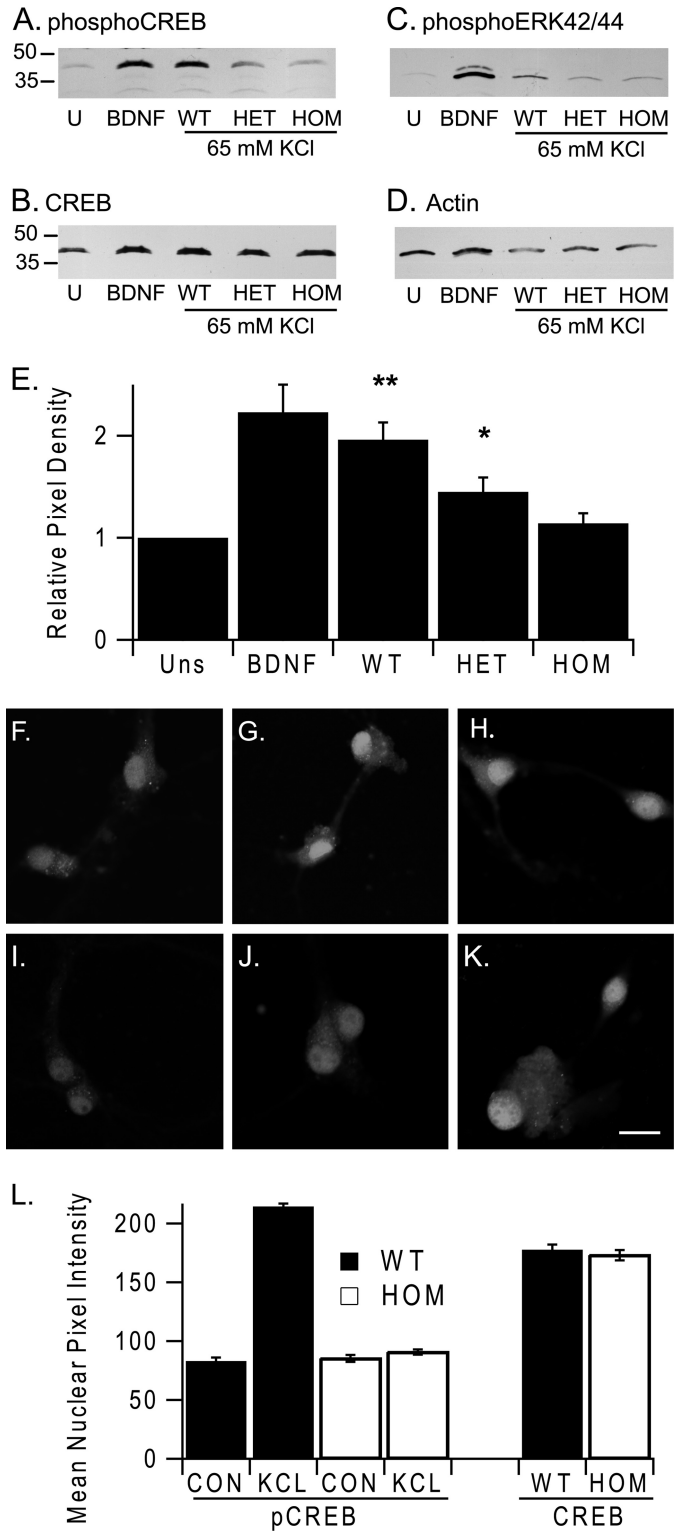

FIGURE 10. **Excitation-transcription coupling in $Ca_V1.2\Delta DCT$ neurons.** CA1/3 hippocampal pyramidal cells were cultured for 8–14 days from wild-type, heterozygous, or homozygous $Ca_V1.2\Delta DCT$ mice. *A–E*, wild-type hippocampal neurons were unstimulated with sham media additions (*U* and *Uns*) or stimulated with brain-derived neurotrophic factor (*BDNF*). Hippocampal neurons from wild-type (*WT*), heterozygous (*HET*), or homozygous (*HOM*) $Ca_V1.2\Delta DCT$ mice were stimulated by depolarization with 65 mM KCl. Samples were lysed in boiling sample buffer, separated by SDS-PAGE, and immunoblotted for phospho-CREB. *A*, phospho-CREB. *B*, total CREB. *C*, phospho-Erk. *D*, actin. *E*, CREB phosphorylation (phospho-CREB/total CREB) normalized to unstimulated cells from experiments analogous to *panel A* (±S.E., $n = 8$) is shown. *F–K*, CA1/3 hippocampal pyramidal cells from wild-type or $Ca_V1.2\Delta DCT$ mice were cultured for 8–14 days. Hippocampal neurons were either unstimulated with a sham medium change or stimulated by depolarization with 65 mM KCl, fixed, and labeled with either total CREB or phospho-CREB antibodies. *F*, WT, pCREB, unstimulated. *G*, WT, pCREB, stimulated with 65 mM KCl. *H*, WT, total CREB. *I*, $Ca_V1.2\Delta DCT$, pCREB, unstimulated. *J*, $Ca_V1.2\Delta DCT$, stimulated with 65 mM KCl. *K*, $Ca_V1.2\Delta DCT$, total CREB. *Scale bars* = 40 μm. *L*, quantification of nuclear staining by phospho-CREB in sham-stimulated and KCl-depolarized cells (*left*) or for total CREB (*right*). Nuclear regions of interest were selected, and mean pixel intensity measured.

of the transcription factor CREB. These three functions of the distal C-terminal domain in the Ca_V1/AKAP signaling complex in neurons are considered in more detail below.

$Ca_V1.2$ Channels Bind AKAP15 in Brain Neurons—Regulation of Ca_V1 channels in skeletal and cardiac myocytes by the β-adrenergic signaling pathway requires PKA anchored to the distal C-terminal domain by AKAP15 (24, 26, 37). Previously, $Ca_V1.2$ channels in neurons were found to interact with the AKAP MAP2B but not with AKAP15 (28). Our results with two different methods of detergent extraction of $Ca_V1.2$ channels show that $Ca_V1.2$ channels are co-immunoprecipitated with AKAP15 and are specifically associated with it. β_2ARs and MAP2B are also associated with $Ca_V1.2$ channels in our co-immunoprecipitation experiments, as expected from previous work (28). These associations are specific because these two neuronal AKAPs, but neither mAKAP nor Yotiao, two other abundant neuronal AKAPs, were detected in our RII-biotin overlay assays. Although all of these proteins are associated with $Ca_V1.2$ channels, our experiments do not determine whether these associations are direct or what fraction of individual $Ca_V1.2$ channels is associated with these kinase anchoring proteins.

$Ca_V1.3$ Channels Form a Signaling Complex with AKAP15 in Brain Neurons—Our results provide the first evidence that AKAP15, MAP2B, and β_2ARs associate with $Ca_V1.3$ channels. The high level of amino acid sequence conservation in the C-terminal region of $Ca_V1.2$ and $Ca_V1.3$ channels suggests that both of these channels bind AKAP15 and are proteolytically processed *in vivo*. Based on our results with $Ca_V1.2$ channels (42) and the high level of conservation of amino acid sequence at the putative cleavage site in the C-terminal domain (41), it is likely that the proteolytically processed distal C-terminal domain of $Ca_V1.3$ remains associated with the channels through noncovalent interactions with the proximal C-terminal domain and serves as a regulator of channel function.

Overlapping Localization of $Ca_V1.2$ and $Ca_V1.3$ Channels with AKAP15—Previous studies have shown that AKAP15 and $Ca_V1.2$ channels closely co-localize in transverse tubule-sarcoplasmic reticulum junctions in skeletal and cardiac muscle (24, 26), but co-localization of $Ca_V1.2$ and $Ca_V1.3$ channels with AKAP15, MAP2B, or β_2ARs has not been studied in neurons. Double-label immunocytochemical studies revealed that AKAP15 has an overlapping localization *in vivo* with $Ca_V1.2$ and $Ca_V1.3$ channels in brain neurons in the cell soma as well as the proximal dendrites and is closely co-localized in punctate clusters of $Ca_V1.2$ channels. These results indicate that a substantial fraction of Ca_V1 channels in the brain have overlapping localization with AKAP15.

In contrast, MAP2B is primarily expressed in distal dendrites and is less extensively co-localized with $Ca_V1.2$ and $Ca_V1.3$

channels in proximal dendrites and in small areas on distal dendrites. MAP2B and AKAP15 have complementary localizations, with AKAP15 present at higher density in cell bodies and proximal dendrites and MAP2B present at higher density in more distal dendritic regions with little somatic staining. These results suggest that these two AKAPs may have complementary roles in localizing PKA in different cellular compartments and that MAP2B may have a more limited role in the regulation of the Ca_V1 channels. Assembly of a β_2AR·$Ca_V1.2$ complex may locally restrict signaling from the receptor to the channel (38), and our results show that β_2ARs interact with both $Ca_V1.2$ and $Ca_V1.3$ channels, supporting a role for highly localized regulation of activity of both channels by β_2ARs.

The Distal C-terminal Domain Is Required for Punctate Localization of AKAP15—If $Ca_V1.2$ channels are a major binding partner of AKAP15, deletion of the distal C-terminal domain with its AKAP15 binding site should prevent the interaction of AKAP15 with $Ca_V1.2$ channels and alter the punctate localization of AKAP15. Using $Ca_V1.2\Delta$DCT mice lacking the distal C terminus, we found that AKAP15 does not co-immunoprecipitate with brain $Ca_V1.2$ channels, in contrast to our results with wild-type littermates. In addition, we observed a substantial change in distribution of AKAP15 from punctate staining to smooth cell surface distribution. These results support the idea that AKAP15 is targeted to the membrane with its lipid anchor but can no longer localize to $Ca_V1.2$ channels because the binding site is unavailable. Evidently, AKAP15 binding to the distal C terminus of $Ca_V1.2$ channels is a major determinant of AKAP15 localization *in vivo*.

The Distal C-terminal Domain Is Required for Normal Functional Expression of $Ca_V1.2$ Channels in Neurons in Vivo—C-terminal truncation of the $Ca_V1.2$ channel results in a 4–6-fold higher calcium channel activity than the full-length form in heterologous expression systems (42, 43), and the co-expressed distal C terminus is a potent inhibitor of channel activity (42, 50). These studies imply that the C terminus exerts an inhibitory effect on calcium current, but these effects of C-terminal truncation have not been determined *in vivo*. In contrast to these expectations from *in vitro* studies, we found that whole-cell L-type calcium currents were diminished in heterozygous and homozygous $Ca_V1.2\Delta$DCT hippocampal neurons. Approximately 30% of the L-type current was lost in heterozygous (HET) $Ca_V1.2\Delta$DCT neurons and ~50% in homozygous (HOM) $Ca_V1.2\Delta$DCT neurons (normalized mean current values: WT, 1.0 ± 0.1; HET, 0.70 ± 0.14; HOM, 0.47 ± 0.08). Inhibition of PKA does not affect basal L-type currents (*e.g.* 51), indicating that reduction of channel activity rather than reduction of basal phosphorylation by PKA is likely to be responsible for this effect. This nearly linear loss of calcium channels in neurons suggests there is no compensatory increase of other Ca_V1 channels that contributes to L-type calcium currents in the homozygous $Ca_V1.2\Delta$DCT mice. These results show that the distal C-terminal is required for normal functional expression of $Ca_V1.2$ channels in neurons *in vivo*.

Studies of $Ca_V1.2$ channels in cardiac myocytes dissociated from the hearts of these E18 $Ca_V1.2\Delta$DCT mice reveal an even greater loss of $Ca_V1.2$ channel protein and $Ca_V1.2$ current (33). Those results suggest a general requirement for the distal C terminus and/or for its proteolytic processing in the functional expression of $Ca_V1.2$ channels in cardiac myocytes.

The Distal C-terminal Domain Is Required for Excitation-Transcription Coupling—Changes in L-type calcium currents lead to sustained activation of CREB through phosphorylation of Ser^{133}. Although L-type calcium currents comprise only 15–20% of the total calcium current in most central neurons, they have a predominant role in regulation of CREB phosphorylation and subsequent gene expression (6, 8, 53). Our experiments with cultured neurons from $Ca_V1.2\Delta$DCT mice show that the distal C-terminal domain of the $Ca_V1.2$ channels is required for normal regulation of CREB phosphorylation in the nucleus, as $Ca_V1.2\Delta$DCT neurons have a nearly complete loss of stimulation of CREB phosphorylation. These results indicate that the distal C-terminal domain of $Ca_V1.2$ channels is critically involved in excitation-transcription coupling *in vivo*.

$Ca_V1.2$ channels also bind AKAP79/150 via LZ interactions with the distal C-terminal domain (54). Interaction of $Ca_V1.2$ channels with the phosphoprotein phosphatase calcineurin through its binding to AKAP79/150 enhances calcium-dependent gene regulation by the nuclear factor of activated T cells (NFAT) and also reduces peak L-type calcium current-conducted $Ca_V1.2$ channels, perhaps as a form of negative feedback regulation of channel activity (54). These results support a key role for the distal C-terminal domain in regulation of gene expression by the NFAT pathway in addition to the CREB pathway.

Recent work suggests that the distal C-terminal domain may serve as a regulator of neuronal gene transcription itself in brain neurons (40). Immunocytochemical and fluorescent-tagging studies detected the distal C-terminal domain in the nuclei of cultured embryonic neurons and a small population of neurons *in vivo*. Transfection of the distal C-terminal domain resulted in nuclear localization and in activation of gene transcription. Our experiments provide further support for this model by showing that the distal C-terminal domain is required for normal activation of CREB *in vivo*. It will be interesting in future studies to determine whether this mechanism plays a pivotal role in long term synaptic plasticity via regulation of gene transcription.

Three Functional Roles for the Signaling Complex Formed by the Distal C terminus of $Ca_V1.2$ Channels in Brain Neurons—Overall, our results point to three previously unrecognized functional roles of the signaling complex formed by distal C-terminal domain of Ca_V1 channels in neurons. The distal C terminus binds AKAP15 and localizes it in punctate clusters with the $Ca_V1.2$ channel itself. The distal C-terminal domain of $Ca_V1.3$ channels has the same function. The distal C-terminal domain is required for normal functional expression of $Ca_V1.2$ channels in brain neurons *in vivo*. The mechanism of this effect may involve altered processing, assembly, and cell surface expression. Finally, the distal C-terminal domain is required for coupling of excitation to phosphorylation of the transcription factor CREB, which may regulate transcription of numerous genes in neurons including the gene encoding $Ca_V1.2$ channels, which is regulated in cardiac myocytes (52). These results establish the distal C terminus as a signaling hub for calcium-dependent regulation of cell function in brain neurons *in vivo*.

Acknowledgments—We thank Dr. Joanne Hulme and Dr. Charles Yokoyama for expert technical assistance and helpful discussions. Additionally, we thank Dr. Marc Grün and Dr. Detlef Hof for help with statistical analysis.

REFERENCES

1. Reuter, H. (1967) *J. Physiol.* **192,** 479–492
2. Reuter, H. (1979) *Annu. Rev. Physiol.* **41,** 413–424
3. Tsien, R. W. (1983) *Annu. Rev. Physiol.* **45,** 341–358
4. Bers, D. M. (2002) *Nature* **415,** 198–205
5. Catterall, W. A. (2000) *Annu. Rev. Cell Dev. Biol.* **16,** 521–555
6. Bading, H., Ginty, D. D., and Greenberg, M. E. (1993) *Science* **260,** 181–186
7. Deisseroth, K., Heist, E. K., and Tsien, R. W. (1998) *Nature* **392,** 198–202
8. Dolmetsch, R. E., Pajvani, U., Fife, K., Spotts, J. M., and Greenberg, M. E. (2001) *Science* **294,** 333–339
9. Finkbeiner, S., and Greenberg, M. E. (1998) *J. Neurobiol.* **37,** 171–189
10. West, A. E., Chen, W. G., Dalva, M. B., Dolmetsch, R. E., Kornhauser, J. M., Shaywitz, A. J., Takasu, M. A., Tao, X., and Greenberg, M. E. (2001) *Proc. Natl. Acad. Sci. U.S.A.* **98,** 11024–11031
11. Weick, J. P., Groth, R. D., Isaksen, A. L., and Mermelstein, P. G. (2003) *J. Neurosci.* **23,** 3446–3456
12. Impey, S., Wayman, G., Wu, Z., and Storm, D. R. (1994) *Mol. Cell Biol.* **14,** 8272–8281
13. Impey, S., Mark, M., Villacres, E. C., Poser, S., Chavkin, C., and Storm, D. R. (1996) *Neuron* **16,** 973–982
14. Hosey, M. M., Barhanin, J., Schmid, A., Vandaele, S., Ptasienski, J., O'Callahan, C., Cooper, C., and Lazdunski, M. (1987) *Biochem. Biophys. Res. Commun.* **147,** 1137–1145
15. Curtis, B. M., and Catterall, W. A. (1984) *Biochemistry* **23,** 2113–2118
16. Curtis, B. M., and Catterall, W. A. (1985) *Proc. Natl. Acad. Sci. U.S.A.* **82,** 2528–2532
17. Takahashi, M., Seagar, M. J., Jones, J. F., Reber, B. F., and Catterall, W. A. (1987) *Proc. Natl. Acad. Sci. U.S.A.* **84,** 5478–5482
18. De Jongh, K. S., Warner, C., and Catterall, W. A. (1990) *J. Biol. Chem.* **265,** 14738–14741
19. Flockerzi, V., Oeken, H. J., Hofmann, F., Pelzer, D., Cavalie, A., and Trautwein, W. (1986) *Nature* **323,** 66–68
20. Hell, J. W., Westenbroek, R. E., Warner, C., Ahlijanian, M. K., Prystay, W., Gilbert, M. M., Snutch, T. P., and Catterall, W. A. (1993) *J. Cell Biol.* **123,** 949–962
21. Westenbroek, R. E., Ahlijanian, M. K., and Catterall, W. A. (1990) *Nature* **347,** 281–284
22. Gross, R. A., Uhler, M. D., and Macdonald, R. L. (1990) *J. Physiol.* **429,** 483–496
23. Gray, R., and Johnston, D. (1987) *Nature* **327,** 620–622
24. Hulme, J. T., Lin, T. W., Westenbroek, R. E., Scheuer, T., and Catterall, W. A. (2003) *Proc. Natl. Acad. Sci. U.S.A.* **100,** 13093–13098
25. Gray, P. C., Tibbs, V. C., Catterall, W. A., and Murphy, B. J. (1997) *J. Biol. Chem.* **272,** 6297–6302
26. Gray, P. C., Johnson, B. D., Westenbroek, R. E., Hays, L. G., Yates, J. R., 3rd, Scheuer, T., Catterall, W. A., and Murphy, B. J. (1998) *Neuron* **20,** 1017–1026
27. Fraser, I. D., Tavalin, S. J., Lester, L. B., Langeberg, L. K., Westphal, A. M., Dean, R. A., Marrion, N. V., and Scott, J. D. (1998) *EMBO J.* **17,** 2261–2272
28. Davare, M. A., Dong, F., Rubin, C. S., and Hell, J. W. (1999) *J. Biol. Chem.* **274,** 30280–30287
29. Snutch, T. P., Tomlinson, W. J., Leonard, J. P., and Gilbert, M. M. (1991) *Neuron* **7,** 45–57
30. Westenbroek, R. E., Hell, J. W., Warner, C., Dubel, S. J., Snutch, T. P., and Catterall, W. A. (1992) *Neuron* **9,** 1099–1115
31. Hell, J. W., Yokoyama, C. T., Wong, S. T., Warner, C., Snutch, T. P., and Catterall, W. A. (1993) *J. Biol. Chem.* **268,** 19451–19457
32. De Jongh, K. S., Murphy, B. J., Colvin, A. A., Hell, J. W., Takahashi, M., and Catterall, W. A. (1996) *Biochemistry* **35,** 10392–10402
33. Fu, Y., Westenbroek, R. E., Yu, F. H., Clark, J. P., III, Marshall, M. R., Scheuer, T., and Catterall, W. A. (2011) *J. Biol. Chem.* **286,** —
34. Westenbroek, R. E., Merrick, D. K., and Catterall, W. A. (1989) *Neuron* **3,** 695–704
35. Westenbroek, R. E., Sakurai, T., Elliott, E. M., Hell, J. W., Starr, T. V., Snutch, T. P., and Catterall, W. A. (1995) *J. Neurosci.* **15,** 6403–6418
36. Westenbroek, R. E., Bausch, S. B., Lin, R. C., Franck, J. E., Noebels, J. L., and Catterall, W. A. (1998) *J. Neurosci.* **18,** 2321–2334
37. Hulme, J. T., Ahn, M., Hauschka, S. D., Scheuer, T., and Catterall, W. A. (2002) *J. Biol. Chem.* **277,** 4079–4087
38. Davare, M. A., Avdonin, V., Hall, D. D., Peden, E. M., Burette, A., Weinberg, R. J., Horne, M. C., Hoshi, T., and Hell, J. W. (2001) *Science* **293,** 98–101
39. Hall, D. D., Davare, M. A., Shi, M., Allen, M. L., Weisenhaus, M., McKnight, G. S., and Hell, J. W. (2007) *Biochemistry* **46,** 1635–1646
40. Gomez-Ospina, N., Tsuruta, F., Barreto-Chang, O., Hu, L., and Dolmetsch, R. (2006) *Cell* **127,** 591–606
41. Hulme, J. T., Konoki, K., Lin, T. W., Gritsenko, M. A., Camp, D. G., 2nd, Bigelow, D. J., and Catterall, W. A. (2005) *Proc. Natl. Acad. Sci. U.S.A.* **102,** 5274–5279
42. Hulme, J. T., Yarov-Yarovoy, V., Lin, T. W., Scheuer, T., and Catterall, W. A. (2006) *J. Physiol.* **576,** 87–102
43. Wei, X., Neely, A., Lacerda, A. E., Olcese, R., Stefani, E., Perez-Reyes, E., and Birnbaumer, L. (1994) *J. Biol. Chem.* **269,** 1635–1640
44. Klöckner, U., Mikala, G., Varadi, M., Varadi, G., and Schwartz, A. (1995) *J. Biol. Chem.* **270,** 17306–17310
45. Abel, T., and Kandel, E. (1998) *Brain Res. Rev.* **26,** 360–378
46. Impey, S., Obrietan, K., Wong, S. T., Poser, S., Yano, S., Wayman, G., Deloulme, J. C., Chan, G., and Storm, D. R. (1998) *Neuron* **21,** 869–883
47. Pittenger, C., Huang, Y. Y., Paletzki, R. F., Bourtchouladze, R., Scanlin, H., Vronskaya, S., and Kandel, E. R. (2002) *Neuron* **34,** 447–462
48. Pizzorusso, T., Ratto, G. M., Putignano, E., and Maffei, L. (2000) *J. Neurosci.* **20,** 2809–2816
49. Zhou, J., Zhang, H., Cohen, R. S., and Pandey, S. C. (2005) *Neuroendocrinology* **81,** 294–310
50. Gao, T., Cuadra, A. E., Ma, H., Bunemann, M., Gerhardstein, B. L., Cheng, T., Ten Eick, R., and Hosey, M. M. (2001) *J. Biol. Chem.* **276,** 21089–21097
51. Endoh, T. (2006) *Br. J. Pharmacol.* **147,** 391–401
52. Schroder, E., Byse, M., and Satin, J. (2009) *Circ. Res.* **104,** 1373–1381
53. Murphy, T. H., Worley, P. F., Nakabeppu, Y., Christy, B., Gastel, J., and Baraban, J. M. (1991) *J. Neurochem.* **57,** 1862–1872
54. Oliveria, S. F., Dell'Acqua, M. L., and Sather, W. A. (2007) *Neuron* **55,** 261–275